Pulsations Along Stellar Evolution
VIII LAPIS Summer School
AAA Workshop Series 12, 2021
M. Kraus & A.F. Torres, eds.

Pulsating Hot Subdwarf Stars

Alejandra D. Romero[1]

[1]*Physics Institute, Universidade Federal do Rio Grande do Sul, Av. Bento Gonçalves 9500, Porto Alegre, RS-91501-970, Brazil*

Abstract. Hot subdwarf stars are core helium–burning objects, located at the hot end of the horizontal branch, and therefore, they are also known as Extreme Horizontal Branch stars. We can divide them into two large groups, of spectral types B and O, depending on their effective temperature. Each spectroscopic class has subgroups showing luminosity variations due to pulsations, opening the possibility to study these compact objects through Asteroseismology. In this notes I will briefly review the main characteristics of hot subdwarfs B and O stars and the different pulsating subgroups.

Key words: asteroseismology — instabilities — stars: oscillations — stars: interiors

1. Introduction

Hot subdwarfs stars are evolved compact stars with temperatures between $\sim 20\,000 - 70\,000$ K and surface gravities ranging from 5.6 to ~ 6.1. They are evolved low mass stars, $M_* < 0.5 M_\odot$, that consist in helium burning cores and a thin hydrogen atmosphere which is unable to support hydrogen shell–burning (Heber et al., 1984; Heber, 1986). They are found in the Galactic field population, classified as type O and B (sdO, sdB), depending on the temperature, and in globular clusters as Extreme Horizontal Branch (EHB) stars.

The progenitors of hot subdwarfs are main sequence stars with initial masses $< 2.0\ M_\odot$, that have undergone a core helium flash and made their way to the Horizontal Branch (HB), with a thin hydrogen envelope ($M_{\rm env} \lesssim 0.01 M_\odot$). As a result of this low hydrogen mass, after core helium exhaustion, the stars move directly to the white dwarf stage.

Around half of hot subdwarf stars are found in binary systems with short periods, from hours to days, with mostly white dwarf companions (Maxted et al., 2001; Napiwotzki et al., 2004; Copperwheat et al., 2011). Since the sdB stars have evolved from red giants, much larger than current orbital separation of a few radii, the progenitor system must have undergone a common envelope (CE) phase.

Subdwarf B and O occupy neighboring regions in the HR diagram. However, they are quite different, both with respect to their chemical compositions and evolutionary status (Heber, 2016). The atmospheres of sdBs are mostly helium poor, their helium abundances might be as low as 1/1000 solar or less. sdO stars,

on the odder hand, show a variety of helium abundances, ranging from 1/100 solar to pure helium atmospheres (He-sdO).

A subgroup of both sdB and sdO stars show luminosity variability due to pulsations. In the case of sdBV there are three classes including the $p-$mode pulsators EC 14026 stars, the $g-$mode pulsators PG 1716 and the hybrid sdBV, showing both $p-$ and $g-$modes. The hotter counterpart, the variable sdO stars show short $p-$mode pulsations. The main characteristics of the classes of pulsating hot subdwarf stars will be addressed in this work.

2. Evolution Towards the Horizontal Branch

The stars in the lower main sequence start their evolution with initial high densities (10^3 g/cm^3 for $\sim 1M_\odot$) and low temperatures, as compared to more massive stars. Thus, at the end of the central hydrogen–burning stage the remaining helium core is close to degeneracy. With the increase in the helium core mass due to the hydrogen burning shell, it soon reaches electron degeneracy conditions, and a new source of pressure is now balancing the gravitational collapse. This structure, of a degenerate core and a non–degenerate envelope is in hydrostatic equilibrium. The hydrogen burning–shell is active and its energy is used to expand the envelope in a giant configuration, thus the star enters the Red Giant Branch (RGB). The effective temperature decreases until it reaches the Hayashi line[1] and then the star starts to increase its luminosity.

The contraction of the core releases gravitational energy that heats up the region where the hydrogen burning–shell is located, also increasing its productivity ($\epsilon_{CNO} \sim T^{20}$). Thus the envelope expands even further, increasing the luminosity.

As the hydrogen–burning shell moves towards the surface of the star, it produces helium increasing the mass of the core. Since the temperature of the core is proportional to its mass ($T \sim M_c/R_c$), it also increases. Thus, when the mass of the core is $\sim 0.45M_\odot$, independently of the total mass of the star, the core reaches a temperature of $\sim 10^8$ K, necessary to start the nuclear reaction of helium. However, since the pressure of the core is dominated by the degenerate electrons, an increase in the temperature due to the release of nuclear reactions does not lead to an expansion of the core. Thus, the expansion work is zero and all the released energy is transformed into internal energy, increasing the temperature even more, leading to an unstable release of energy. The large amount of energy is released fast as compared to evolution timescales, in an event called the helium–flash (He–flash). The energy produced in the core by the He–flash can reach luminosity of $10^{10}L_\odot$ comparable to the luminosity of our Galaxy. Finally, the temperature will increase until $T > T_{\rm Fermi}$ and the pressure depends on the temperature again. The core expands and cools, and the stable nuclear burning stage begins, i.e. the Horizontal Branch.

---

[1]The Hayashi line marks the lowest effective temperature than can be reached by a stable configuration. The line itself corresponds to a fully convective star.

3. The Formation of Extreme Horizontal Branch Stars

Hot subdwarf stars are located at the hot end of the Horizontal Branch, characterized by a hydrogen envelope too thin to support nuclear shell–burning. The main issue to understand the formation of EHB stars is the large amount of mass that needs to be lost prior to or at the beginning of core helium burning. Two main formation channels have been proposed, being close binary evolution or the hot flasher scenario. Binary evolution through mass transfer and common envelope ejection must be important for sdB stars due to the high percentage of close binaries with periods of less than ten days. In addition, merger of two helium white dwarfs is another vital option to explain the origin of single hot subdwarfs. Enhanced mass loss during the RGB can decrease the hydrogen content of the envelope, delaying the core helium flash (the so-called *hot flasher scenario*), during which surface hydrogen is burnt after mixing into deeper layers (Heber, 2016). More detail on the possible formation channels are given below.

3.1. Hot Flasher Scenario

Stars corresponding to the low main sequence, where hydrogen burning is mainly due to the $p-p$ cycle, begin the central helium burning stage with the He–flash at the tip of the RGB. However, if sufficient mass loss occurs during the RGB, the star will experience the He–flash at higher effective temperatures (Castellani & Castellani, 1993). The remnants of these "hot flashers" (Brown et al., 2001) are found to be close to the helium main sequence. The outcome of a hot flasher depends on the evolutionary phase during which it occurs (Cassisi et al., 2003), as shown in Figure 1. Panel (a) shows the evolution where the mass loss was slightly enhanced. In this case, the He–flash occurs near the tip of the RGB and the star settles near the blue horizontal branch. If the He–flash occurs early after departure from the RGB (*Early hot flasher*) at high luminosities and effective temperatures, the further evolution results in a standard H/He envelope hot subdwarf star (see panel b in Figure 1). The *Late hot flasher* scenario occurs when the He–flash happens after the star enters the white dwarf cooling sequence. If the He–flash occurs at high $T_{\rm eff}$, there is shallow mixing, resulting in a hot subdwarf star with an atmosphere enriched in helium and nitrogen due to convective dilution of the envelope (see panel c in Figure 1). If the He–flash occurs at a lower luminosity in the white dwarf cooling sequence (see panel d in Figure 1), the hydrogen–rich envelope is mixed and burned in the convective zone generated by the flash itself leading to strong enrichment of helium, carbon and nitrogen in the atmosphere (Heber, 2009, 2016; Battich et al., 2018). Thus, when in the evolution the He–flash occurs, it not only determines the effective temperature of the star on the EHB but also its envelope chemical composition.

3.2. Close Binary Evolution

The large fraction of sdB stars in close binaries suggests that they are formed by binary interaction. There are three main formation channels: Roche–lobe overflow (RLOF) evolution, common envelope (CE) evolution (Paczynski, 1976), and the merger of two he–core white dwarfs (Webbink, 1984; Han et al., 2002, 2003).

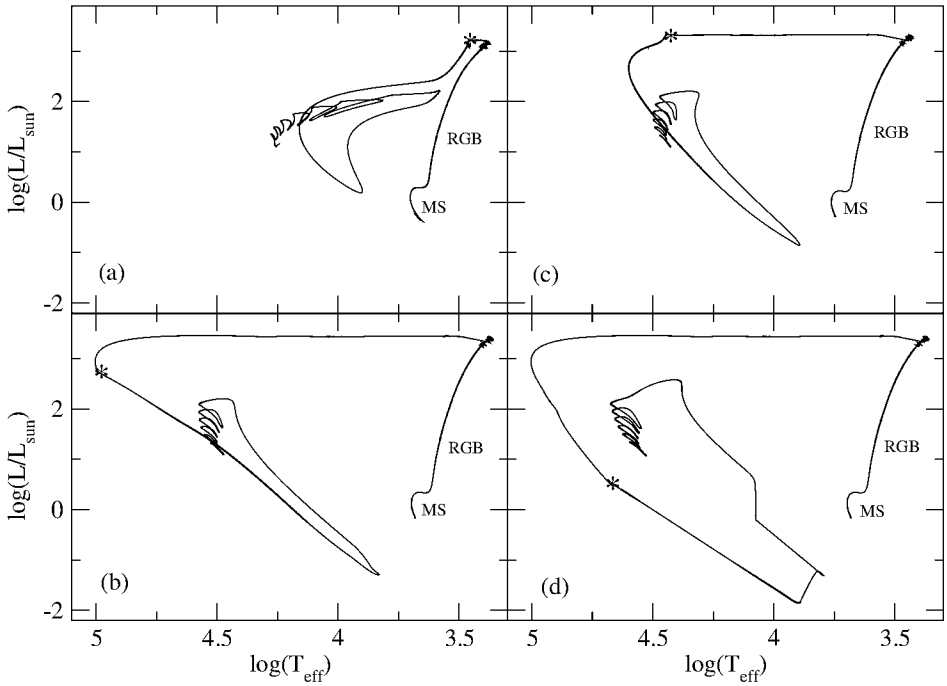

Figure 1. Evolution of a solar metallicity star from the main sequence to the zero–age horizontal branch for different mass loss rates on the RGB. The peak of the He–flash is indicated with a blue asterisk. (a) The He–flash occurs soon after the tip of the RGB. (b) *Early hot flasher*: the He–flash occurs at high luminosities and effective temperatures. (c) *Late hot flasher*: The He–flash occurs soon after entering the white dwarf cooling curve, causing a shallow mixing episode. (d) *Late hot flasher*: The He–core occurs during the white dwarf cooling sequence causing a deep mixing episode. Credit: The evolutionary sequences from panels b, c and d were provided by Tiara Battich (private communication), Battich et al. (2018).

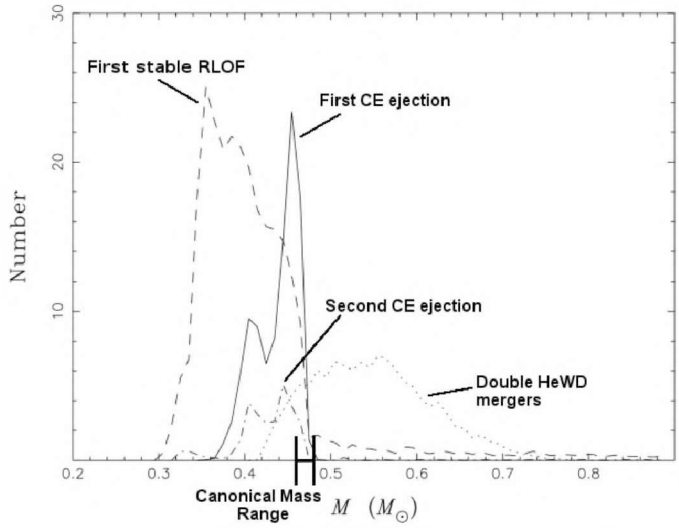

Figure 2. Contribution of the different close binary formation channels to the population of hot subdwarf stars. Credit: Adapted by Ingrid Pelisoli from Han et al. (2003).

In the RLOF formation channel, the mass transfer is dynamically stable and the companion star accretes all the matter. The red giant loses almost all its hydrogen–rich envelope during this stage and becomes a sdB star in a long period binary with a main sequence component. The orbital periods are in the range of 700–1300 days (Chen et al., 2013).

In the CE formation channel, the sdB progenitor fills its Roche lobe near the tip of the RGB. If the mass transfer rate is too high, the companion will not be able to accrete all the material, forming a common envelope. Due to friction with the gas the system will lose orbital energy and the orbit will shrink. The orbital energy is transferred to the common envelope until it is enough to eject it. The remaining core of the red giant will become the sdB star. Because the CE phase is short as compared to the evolutionary timescale of the single stars, the companion will remain almost unchanged. If the companion is a main sequence star the resulting close binary is a sdB+MS with a period between 0.1 and 10 days (Heber, 2016). Even with the current advances in modeling, the physics behind common envelope and accretion is not well understood. Recent works as Davis et al. (2010) and Toonen & Nelemans (2013) are aimed at explaining the formation of white dwarf binaries, while Clausen et al. (2012) is focused on sdB binaries (Heber, 2016).

The most popular formation channel for single hot subdwarfs is the merger of two helium core white dwarf stars (Webbink, 1984). The merger scenario can be slow, fast or a combination of both (Zhang & Jeffery, 2012). In the slow merger scenario the largest star, i.e. the less massive white dwarf, fills its Roche lobe and all the mass is transferred to the companion. The material will form a disk in a few minutes and it will remain cold. The accretion is slow and can last for a few million year, with the angular momentum being dissipated towards

the disk circumference. On the other hand, in the fast merger scenario, no disk is formed and the material falls directly onto the surface of the more massive, smaller companion. A combination of both scenarios is also possible, where one part of the disrupted donor star forms a corona (30%-50% of its mass), and the rest forms a cold disk (Zhang & Jeffery, 2012; Lorén-Aguilar et al., 2009).

Each channel contributes to the population of hot subdwarfs in different amounts and mass range. Han et al. (2003) carried out a detailed binary population synthesis study considering CE and RLOF formation channels. In particular, they predicted that the distribution of masses for sdB stars is wider than is commonly assumed, with stellar masses ranging from 0.3 to $\sim 0.8 M_{\odot}$, as shown in Figure 2. The canonical mass range, indicated in the figure, corresponds to the contribution from the hot flasher scenario. This result is in very good agreement with the distribution of the current population of hot subdwarf stars shown by Schneider (2019)[2], where the mass range can be as low as $0.2 M_{\odot}$ and larger than $0.7 M_{\odot}$ in a few cases. There is a large contribution of objects near $\sim 0.4 M_{\odot}$, that also have contributions from the hot flasher scenario, and a tail at lower masses that can only be formed through binary interaction.

4. Chemical Structure and the Characteristic Frequencies

Hot subdwarf stars are part of the Extreme Horizontal Branch stage, where helium in the core is being transformed into carbon and oxygen due to nuclear reactions. At first, nuclear energy is being produced through the 3α process, where three nuclei of helium, or α particles, are combined to form a carbon nucleus. Once the abundance of carbon in the convective core is high enough, $\sim 50\%$, the reaction $^{12}\mathrm{C}(\alpha,\gamma)\mathrm{O}^{16}$ starts to be dominant, since it is more likely to combine two particles than three. Thus, the carbon abundance reaches a maximum and then decreases, along with the helium abundance. As a result, the star leaves the horizontal branch with a carbon/oxygen core, usually with $\mathrm{C/O} < 1$.

The chemical profile of a hot sdB model with stellar mass $0.474 M_{\odot}$, and $T_{\rm eff} = 26\,214$ K is shown in Figure 3. In this figure only the more abundant elements are depicted. As expected, the central regions are a mixture of carbon, oxygen and helium. Carbon is still dominant but eventually its abundance will decrease and oxygen will become the dominant element. The helium rich region on top of the core is the remnant from hydrogen burning during the main sequence, since the He–burning core is always smaller than the H-burning regions. Finally, no diffusion was considered in the computations, thus the envelope is a mixture of helium and hydrogen.

Each chemical transition in the inner structure, will lead to a distinctive signature in the characteristic frequencies for pulsation. In Figure 4 we show the propagation diagram for an sdB model with stellar mass $0.473 M_{\odot}$, $T_{\rm eff} = 28\,700$K and $\log g = 5.53$. The full line corresponds to the run of the Brunt-Väisaälä frequency (N^2), while the dashed curve is the run of the Lamb frequency (L_ℓ) for $\ell = 2$. The gray shaded region corresponds to the evanescence region.

[2]https://zenodo.org/record/3428841#.XcWlWJLYpE4

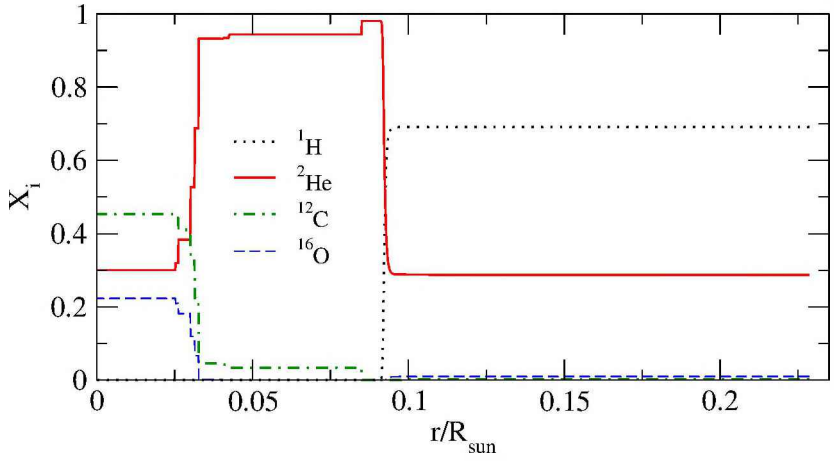

Figure 3. Chemical abundance as a function of radius for a sdB model of $0.474 M_{\odot}$, and $T_{\rm eff} = 26\,214$ K. Only the most abundant elements are depicted.

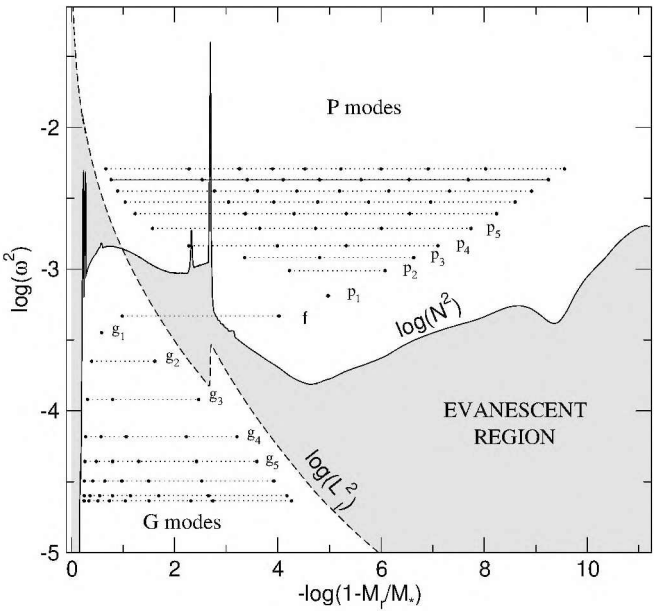

Figure 4. Propagation diagram for a sdB model with $0.473 M_{\odot}$, and $T_{\rm eff} = 28\,700$ K, for $\ell = 2$ modes. The Brunt-Väisälä (full line) and Lamb (dashed line) frequencies are also depicted, separating the propagation and evanescent regions. The horizontal lines show the square values of the eigenfrequencies and the circles mark the position of the nodes in the radial eigenfunction.

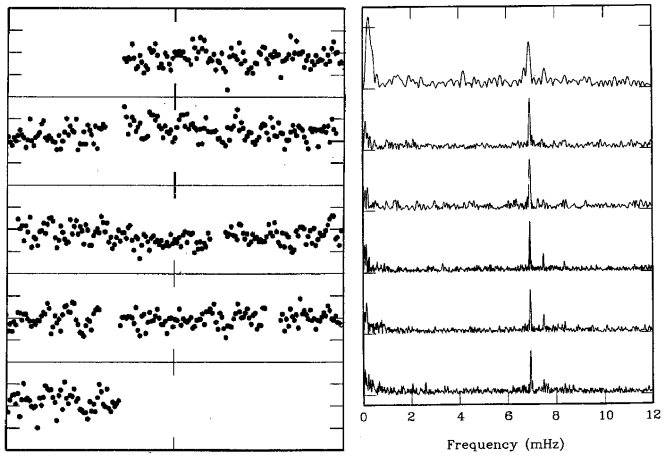

Figure 5. Light curve (left) and Fourier Transform (right) EC 14026-2647 for the original data from Kilkenny et al. (1997). The ordinate in the light curve are separated by 0.05 mag and the abscissae by 0.01 d, so that the data read continuously from left to right and top to bottom, from fractional Julian date 0.307 to 0.387. For the FT the ordinate carets are separated by 0.015 mag. Credit: Kilkenny et al. (1997).

Propagation is possible if the frequency of the mode is higher or lower than N^2 and L_ℓ. Modes in the region of high frequency correspond to pressure modes while gravity modes are found in the low frequency regions (Unno et al., 1979). As can be seen from Figure 4, pressure modes propagate in regions closer to the surface while gravity modes will show larger amplitudes in the inner regions of the star. This effect is better depicted by the horizontal lines showing the square values of the eigenfrequencies and the circles marking the position of the nodes in the radial eigenfunction (y_1). Thus, p–modes will bring information on the outer layers while g–modes will bring information on the central regions.

5. Pulsating Subdwarf B Stars

The first pulsating sdB was discovered by Kilkenny et al. (1997) with the South African Observatory, EC 14026-2647, showing short period variability with a main period around $\sim$ 144 s. Therefore, this class of variable sdB is known as EC 14026. The light curve and Fourier Transform are presented in Figure 5. Independently and almost at the same time, Charpinet et al. (1996) predicted the existence of pulsation instability for pressure modes in sdB stars, due to the classical κ-mechanism associated to the $Z-$peak in the opacity. Figure 6 shows the run of the Rosseland opacity compared to the time derivative of the work function dW/dr for the fundamental mode with $\ell = 2$ (Charpinet et al., 1996). The peak in dW/dr is directly related to the peak in the opacity due to heavy elements marked as "Z-bump". Charpinet et al. (1996) first found that instability was only present for high metallicity models with $Z > 0.04$, but in a later work (Charpinet et al., 1997) they found that the enhancement in

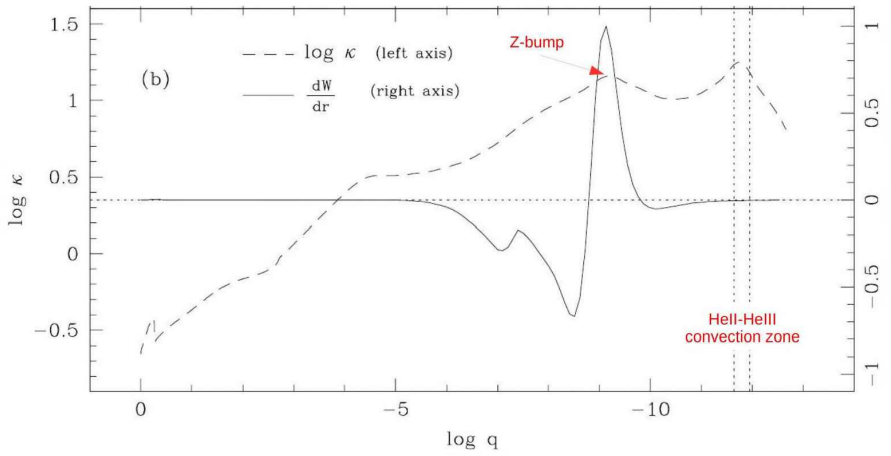

Figure 6. Run of the Rosseland opacity (dashed line) and the integrand of the work integral for the fundamental mode with $\ell = 2$ (solid line). Driving regions ($dW/dr > 0$) are clearly associated with the opacity bump, caused by heavy element ionization (Z-bump). The HeII-HeIII convection zone is indicated with vertical dotted lines. Credit: Charpinet et al. (1996), © AAS. Reproduced with permission.

the Fe–peak elements in the driving region was enough to drive pulsations. The local overabundance of heavy elements is possible due to the equilibrium between radiative levitation and gravitational settling processes.

EC 14026, also called V361 Hya stars, pulsate in pressure modes with short periods between 80 s and 580 s, with amplitudes of $0.3 - 64$ mmag. They are found mainly among the hotter sdBs, with effective temperatures between 28 000 and 35 000 K, and $\log g \sim 5.8$. The position of the current sample of EC 14026 stars in the $\log g - T_{\rm eff}$ plane is depicted in Figure 7 (blue circles) in the low $\log g$ part of the diagram, along with all classes of pulsating hot subdwarfs, that will be discussed below. The data was extracted from Table 1 of Holdsworth et al. (2017). The sdB instability strip is not pure, and around 10% of the objects in the temperature range where EC 14026 stars are found, show pulsations (Østensen et al., 2010).

The second class of variable sdB stars was discovered by Green et al. (2003). These stars are known as V1093 Her, or PG 1716 after the prototype PG 1716+426. PG 1716 stars are long period pulsators with periods between 1400 and 43 500 s, and amplitudes of $0.4 - 4.1$ mmag. As can be seen from Figure 7 (red triangle–up), they are cooler than the p-mode pulsators EC 14026, with effective temperatures between 23 000 and 30 000 K, and $\log g \sim 5.4$. Fontaine et al. (2003) showed that g-mode pulsations are excited in PG 1716 stars by the same κ-mechanism proposed by Charpinet et al. (1996, 1997), if the observed g-modes are high radial order and high harmonic degree ($\ell \geq 3$) modes. Around %75 of the objects inside the PG 1716 instability strip show brightness variations.

Three years later, Schuh et al. (2006) reported the first pulsating sdB, HS 0702+6043, that showed both short and long periods, and thus it was called a

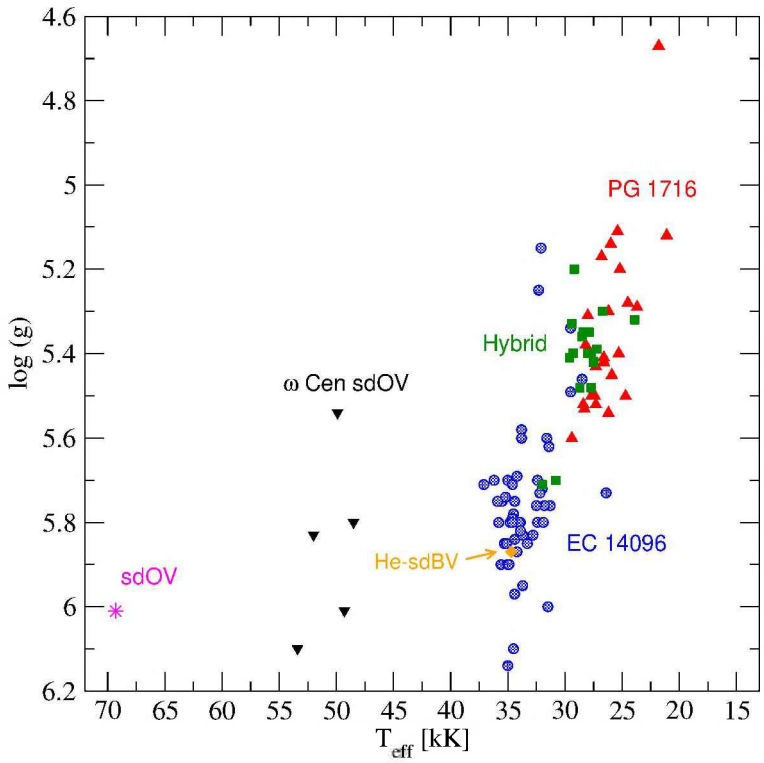

Figure 7. The distribution of the variable hot subdwarf stars in the $\log g - T_{\rm eff}$ plane. Each class is indicated with different symbols and colors. The sub-classes of sdBV stars EC 14026 (blue circles), PG 1716 (red up triangle) and the Hybrid (green squares) are depicted in the low temperature part of the plane. The only He-sdBV is also included (orange diamond). SdO variables are located in the hot part of the diagram, the only sdOV detected in the field of the Galaxy (magenta star) and those discovered in the globular cluster ω Cen (black down triangle). The values of $\log g$ and effective temperatures where taken from Table 1 of Holdsworth et al. (2017).

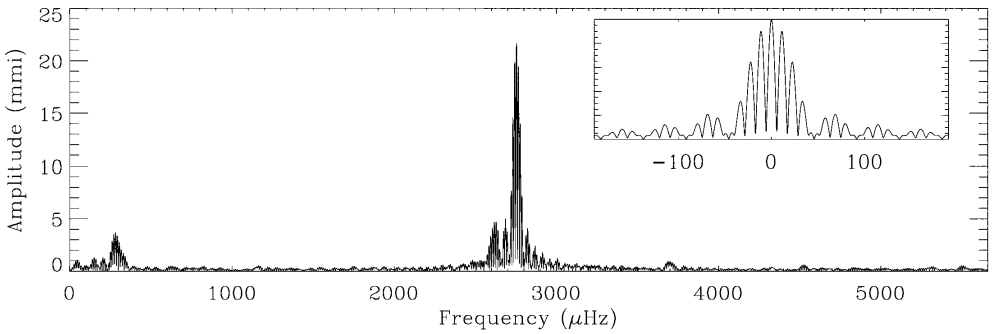

Figure 8. Fourier transform for the discovery of the hybrid sdB star HS 0702+6043. The plot shows the Fourier Transform of the full light curve, with the window function for the two–night data set displayed in the inset panel in the upper right corner (frequency in μHz as in the main plot, the amplitude scaling is arbitrary). Credit: Schuh et al. (2006). Copyright A&A. Reproduced with permission © ESO.

hybrid sdBV star. HS 0702+6043 was previously identified as a EC 14026 star with two short periods of 363 s and 383 s, but further observations revealed a low–amplitude ($\sim$ 4 mmag), long–period of 3538 s, identified by Schuh et al. (2006) as a g-mode pulsation. The Fourier Transform from Schuh et al. (2006) is shown in Figure 8. Hybrid sdBV stars show effective temperatures $\sim$ 28 000 K, between long and short period sdBVs, as it is shown in Figure 7, where hybrid sdBVs are depicted with green squares. Since $p-$modes propagate in the outer regions of the star, whereas $g-$modes do in the deep interior, the whole internal structure of the star can be sampled in the case of hybrid sdB stars (Heber, 2016).

The only pulsating He–sdBV is also depicted in Figure 7 (orange diamond). He–sdB stars are a very small group of subdwarf stars that show varying degrees of helium enrichment in the envelope, but have effective temperatures similar to hydrogen rich sdB stars (Ahmad & Jeffery, 2003). Variability of the He-sdBV, LV IV–14° 116, was reported by Ahmad & Jeffery (2003), with the detection of two long periods of 1953 s and 2870 s, characteristic of g–mode pulsations.

The period range for each class of pulsating sdB stars is shown in Figure 9, where the period range for all sdB stars from Figure 7 are depicted in the Period–log g plane. EC 14026 $p-$mode pulsators show periods in the range of 60–600 s, while PG 1716 $g-$mode pulsators show long periods in the range of 1400–44000 s. Hybrids are in between, with periods in the range of 118–28500 s.

6. Pulsating Subdwarf O Stars

Subdwarf O stars are intrinsically hotter than sdB stars. In addition, they show a range of helium abundance in the atmosphere, from a hundredth of solar content to pure helium. As an example, Figure 10 shows the normalized spectra of the sdO J16007+0748 (Woudt et al., 2006). The He II lines are clearly present in

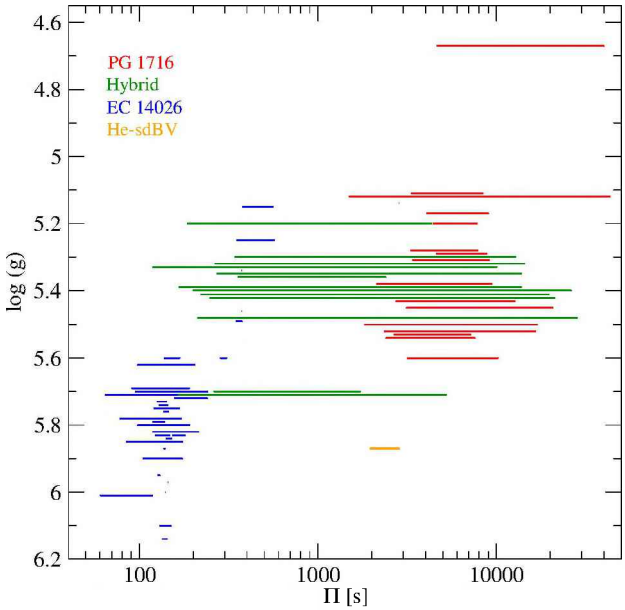

Figure 9. Period-log g diagram for the pulsating sdB stars presented in Figure 7. The colors represent the same as the previous figure. The data was taken from Table 1 of Holdsworth et al. (2017).

absorption, along with the Balmer series lines from $H\beta$ to $H\epsilon$. Given the small binary fraction of sdO stars, merger of two helium white dwarfs or hot flasher evolution are the most likely formation channels.

J16007+0748 is the first and only pulsating sdO in the Galactic field. Woudt et al. (2006) reported the detection of short period variability with a main period of 119.33 s, being identified with p–mode pulsations. The position of the sdOV is depicted in Figure 7 with a magenta star, being the hottest object of the sample.

Latter, Randall et al. (2010, 2011) reported the detection of four sdOV stars in the globular cluster ω Cen. The objects showed periods in the range between 84 s and 119 s, in agreement with the sdOV found by Woudt et al. (2006). Currently, there are five sdOV stars from ω Cen, depicted with black down–triangles in Figure 7. Contrary to the sdOV star found in the field, the objects belonging to the globular cluster, show hydrogen dominated atmospheres, and are also cooler. This could be related to the lower metallicity of the cluster as compared to the disk population. The excitation mechanism seems to be $\kappa-$mechanism, similar to sdBV stars (Randall et al., 2016).

7. Concluding Remarks

In this work I briefly described the main characteristics of the pulsating hot subdwarf stars. I recommend the excellent reviews of Heber (2009) and Heber (2016) and references therein, for more details.

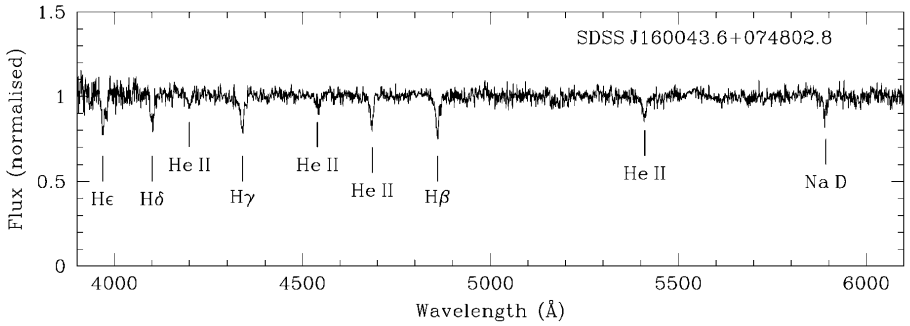

Figure 10. Combined SALT spectrogram of J16007+0748 (only sdOV star) obtained with a total exposure time of 1800 s. The absorption lines are marked and labelled. Credit: Woudt et al. (2006).

There are currently, $\sim$ 100 sdB variables and six sdO variables reported (Holdsworth et al., 2017), including those found with *Kepler* satellite observations. New space and ground-based surveys are expected to increase this sample. In particular the *TESS* (*Transit Exoplanet Survey Satellite*) is a great tool to find bright variables, as hot subdwarf stars, with around 40 confirmed objects.

It is important to notice that, in order to study hot subdwarf stars using asteroseismology, physically sound representative models should be available, in order to compare the observed periods with theoretical pulsation spectrum. In particular, by studying the inner structure of hot subdwarf stars we could shed some light on the formation channels of these compact blue objects.

Acknowledgments. We would like to thank Larissa Antunes Amaral, Maja Vučković and Murat Uzundag for their help in preparing the presentation.

References

Ahmad A., Jeffery C. S., 2003, *A&A*, **402**, 335
Battich T., Miller Bertolami M. M., Córsico A. H., Althaus L. G., 2018, *A&A*, **614**, A136
Brown T. M., Sweigart A. V., Lanz T., Land sman W. B., Hubeny I., 2001, *ApJ*, **562(1)**, 368
Cassisi S., Schlattl H., Salaris M., Weiss A., 2003, *ApJL*, **582(1)**, L43
Castellani M., Castellani V., 1993, *ApJ*, **407**, 649
Charpinet S., Fontaine G., Brassard P., Chayer P., Rogers F. J., Iglesias C. A., Dorman B., 1997, *ApJL*, **483(2)**, L123
Charpinet S., Fontaine G., Brassard P., Dorman B., 1996, *ApJL*, **471**, L103
Chen X., Han Z., Deca J., Podsiadlowski P., 2013, *MNRAS*, **434(1)**, 186
Clausen D., Wade R. A., Kopparapu R. K., O'Shaughnessy R., 2012, *ApJ*, **746(2)**, 186
Copperwheat C. M., Morales-Rueda L., Marsh T. R., Maxted P. F. L., Heber U., 2011, *MNRAS*, **415(2)**, 1381
Davis P. J., Kolb U., Willems B., 2010, *MNRAS*, **403(1)**, 179

Fontaine G., Brassard P., Charpinet S., Green E. M., Chayer P., Billères M., Rand all S. K., 2003, *ApJ*, **597(1)**, 518
Green E. M., Fontaine G., Reed M. D., Callerame K., Seitenzahl I. R., White B. A., Hyde E. A., Østensen R., Cordes O., Brassard P., Falter S., Jeffery E. J., Dreizler S., Schuh S. L., Giovanni M., Edelmann H., Rigby J., Bronowska A., 2003, *ApJL*, **583(1)**, L31
Han Z., Podsiadlowski P., Maxted P. F. L., Marsh T. R., 2003, *MNRAS*, **341(2)**, 669
Han Z., Podsiadlowski P., Maxted P. F. L., Marsh T. R., Ivanova N., 2002, *MNRAS*, **336(2)**, 449
Heber U., 1986, *A&A*, **155**, 33
Heber U., 2009, *ARA&A*, **47(1)**, 211
Heber U., 2016, *PASP*, **128(966)**, 082001
Heber U., Hunger K., Jonas G., Kudritzki R. P., 1984, *A&A*, **130**, 119
Holdsworth D. L., Østensen R. H., Smalley B., Telting J. H., 2017, *MNRAS*, **466(4)**, 5020
Kilkenny D., Koen C., O'Donoghue D., Stobie R. S., 1997, *MNRAS*, **285(3)**, 640
Lorén-Aguilar P., Isern J., García-Berro E., 2009, *A&A*, **500(3)**, 1193
Maxted P. F. L., Heber U., Marsh T. R., North R. C., 2001, *MNRAS*, **326(4)**, 1391
Napiwotzki R., Karl C. A., Lisker T., Heber U., Christlieb N., Reimers D., Nelemans G., Homeier D., 2004, *Ap&SS*, **291(3)**, 321
Østensen R. H., Oreiro R., Solheim J. E., Heber U., Silvotti R., González-Pérez J. M., Ulla A., Pérez Hernández F., Rodríguez-López C., Telting J. H., 2010, *A&A*, **513**, A6
Paczynski B., 1976, P. Eggleton, S. Mitton, and J. Whelan (eds.), *Structure and Evolution of Close Binary Systems*, Vol. 73 of *IAU Symposium*, p. 75
Randall S. K., Calamida A., Bono G., 2010, *Ap&SS*, **329(1-2)**, 55
Randall S. K., Calamida A., Fontaine G., Bono G., Brassard P., 2011, *ApJL*, **737(2)**, L27
Randall S. K., Calamida A., Fontaine G., Monelli M., Bono G., Alonso M. L., Van Grootel V., Brassard P., Chayer P., Catelan M., Littlefair S., Dhillon V. S., Marsh T. R., 2016, *A&A*, **589**, A1
Schuh S., Huber J., Dreizler S., Heber U., O'Toole S. J., Green E. M., Fontaine G., 2006, *A&A*, **445(3)**, L31
Toonen S., Nelemans G., 2013, *A&A*, **557**, A87
Unno W., Osaki Y., Ando H., Shibahashi H., 1979, *Astronomy Quarterly*, **3**, 197
Webbink R. F., 1984, *ApJ*, **277**, 355
Woudt P. A., Kilkenny D., Zietsman E., Warner B., Loaring N. S., Copley C., Kniazev A., Väisänen P., Still M., Stobie R. S., Burgh E. B., Nordsieck K. H., Percival J. W., O'Donoghue D., Buckley D. A. H., 2006, *MNRAS*, **371(3)**, 1497
Zhang X., Jeffery C. S., 2012, *MNRAS*, **419(1)**, 452